

MEASUREMENT OF ELASTIC STRAINS IN CRYSTAL SURFACES BY X-RAY DIFFRACTION TOPOGRAPHY

Brian R. Lawn*

*Division of Engineering
Brown University
Providence, Rhode Island*

ABSTRACT

The use of X-ray topographic techniques for studying elastic strains in crystals deformed at their surfaces is becoming widespread, especially in the field of silicon semiconductor devices. Although the broad features of the phenomenological processes involved in producing the strain patterns on the X-ray micrographs are understood, little attention has been devoted to evaluating the detailed nature or range of the strain fields in the crystal. In this paper, an elastic model is proposed for cases in which a region of crystal surface is uniformly deformed over a thin layer. With this model, the associated strain field in the surrounding crystal, which is readily computed from elasticity theory, may be characterized by a single parameter. The model is in accord with observed strain patterns on topographs of abraded diamond surfaces and silicon surfaces onto which a strip of metal film has been evaporated. From the spatial range of the diffraction contrast, an estimate of the parameter characterizing the strain field may be made.

INTRODUCTION

In recent years, the methods of X-ray topography have found increasing application in the study of elastic strains in crystal surfaces. Such strains may be introduced by any process which deforms the crystal surface and thus leaves it in a state of residual stress. Partial relief of the residual stress is then manifested as an elastic distortion of the crystal matrix surrounding the deformed region of surface, provided, of course, no plastic flow occurs. The edges of metal strips evaporated onto silicon substrates¹ and the boundaries of parts of crystal surface damaged by mechanical abrasion,² particle or photon irradiation,³ or chemical effects such as surface diffusion and oxidation^{1,4} are examples of regions where elastic strain fields have been detected by X-ray diffraction contrast. The existence of this type of strain field is of interest from a practical as well as an academic standpoint. For instance, the presence of the elastic strains at the edges of evaporated thin films is believed to be an instrumental factor in the breakdown of semiconductor devices.

Most attention in the studies performed to date has been directed toward a basic understanding of the physical processes causing the elastic strains and to a qualitative interpretation of the associated diffraction contrast on the topographs. This paper is concerned more with the nature and magnitude of the elastic strain field itself. An elastic model is first proposed in which the strain field can be calculated and characterized by a single parameter. The diffraction contrast on X-ray topographs is then examined and used to verify the essential predictions of the model. Finally, from a measurement of the

* Present address: School of Physics, University of N.S.W., Kensington, N.S.W., Australia.

range of observable diffraction contrast, an estimate of the characterizing strain parameter is made.

ELASTIC MODEL

In the interest of simplicity, we specify the following assumptions: (1) The strains in the matrix crystal are taken to be representable by the equations of linear isotropic elasticity; (2) the depth δ of the deformed surface layer of crystal is assumed small compared to the surface dimensions of the layer, which are in turn assumed small compared to the dimensions of the crystal itself; (3) the deformation is considered uniformly distributed throughout the deformed region of crystal at the surface. Thus, we have as our model an otherwise perfect semi-infinite crystal matrix with a thin isotropic layer of "bad" crystal embedded in its surface.

The strain field in crystal surrounding a deformed surface layer of arbitrary shape may now be computed in the following manner. Let us consider the residual stress in the bad layer compressive (tension will simply reverse the sign of the strains) so that the layer must expand to relieve the stresses. Since δ is small, this tendency to expand will give rise to an outwardly directed normal pressure p , very nearly parallel to the crystal surface, on the matrix at the peripheral boundary of the layer. By Saint-Venant's principle, as long as we do not concern ourselves with the strain situation within distances δ of the periphery, we may consider the pressure p equivalent to a line force F per unit of length of the periphery. Writing \mathbf{n} as a unit vector lying in the crystal surface and directed perpendicularly outward from the periphery of the bad layer (Figure 1), we then have $\mathbf{F} = p\delta\mathbf{n}$. Defining a system of cartesian coordinates by the unit vectors $\mathbf{x}_1, \mathbf{x}_2, \mathbf{x}_3$, we can now compute the displacements at any point (x_1, x_2, x_3) in the crystal owing to an effective point force Fdl at $(x'_1, x'_2, 0)$ and, by integrating around the entire periphery of the bad layer, the total displacement field may be determined. Following Landau and Lifshitz,⁵ we arrive at an expression of the following type for the i th component of the displacement vector:

$$u_i = \frac{F}{E} \oint G_{ik}(x_1 - x'_1, x_2 - x'_2, x_3, \nu) n_k dl \quad (1)$$

where E is Young's modulus; ν is Poisson's ratio; n_k is the component of \mathbf{n} in the direction \mathbf{x}_k ; the G_{ik} are given by Landau and Lifshitz;⁵ and k is a repeated suffix. In equation (1), F is assumed constant everywhere on the periphery (this assumption demands further consideration in special instances). From equation (1), the strain field may be established for any shape of periphery of bad crystal. A high-speed computer is generally required to perform the calculations. Such calculations have been done for elliptical microabrasion patches on surfaces of diamond.²

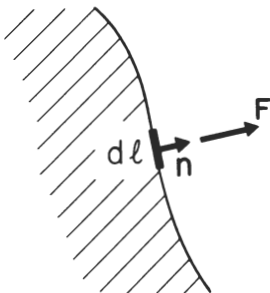


Figure 1. The force exerted by a deformed surface layer on a crystal matrix.

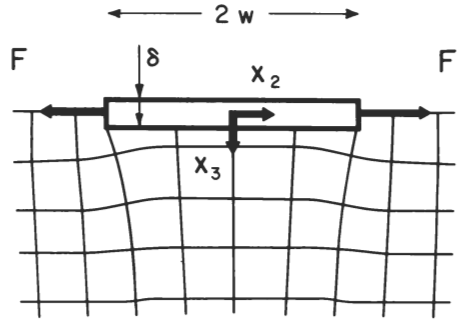


Figure 2. Distortion of the crystal lattice due to residual compressive stress in the deformed layer.

In the present paper, we can choose a particularly simple peripheral geometry without loss in generality. We take the bad layer to be a long strip parallel to \mathbf{x}_1 with edges at $x_2 = \pm w$ and thickness δ measured in direction x_3 . Such a description probably applies reasonably well to the strips of metal evaporated onto silicon surfaces.¹ Solutions for the strain field may be computed from equation (1) or, alternatively (for this particular case) from the two-dimensional solution for straight-line forces in a surface given by Timoshenko and Goodier⁶ and others. The expressions for the displacements and strains are too cumbersome to be given here. Instead, the displacements are displayed in schematic form in Figure 2 as a distorted lattice for an arbitrary value of F .

SOME VERIFICATIONS OF THE MODEL

The object of this section is to provide evidence supporting the model outlined in the previous section.

Optical Examination of the Crystal Surface

One of the predictions of the elastic model is readily investigated by optical means. As seen in Figure 2, the crystal surface surrounding the embedded bad layer is flat, a prediction which turns out to be independent of the peripheral shape of the layer. The crystal surfaces surrounding elliptical abrasion patches on diamond and evaporated metal strips on silicon are indeed found to be flat (allowing for original surface roughness) within the limits of detection of interference microscopy. The model similarly predicts that the central, deformed region of the surface will be raised or lowered slightly according to whether the direction of \mathbf{F} is outward or inward, but the very nature of the deforming mechanism precludes any observation of such an effect in the cases studied here. In the case of the abraded diamond, some material is removed from the surface, and, in the case of the metal strip on the silicon substrate, the thickness of the evaporated strip obscures any measurement. However, in the latter case, the top surface of the strip is found to be flat, as the model would predict for a uniformly thick layer.

X-Ray Topographs of the Crystals

The optical examinations mentioned above provide no indication that the crystal might be in a state of residual strain. However, the extremely strain-sensitive techniques of X-ray topography⁷ reveal quite plainly the presence of the strain field, as seen in Figures 3 and 4 (taken under the usual experimental arrangement in which the angular divergence of the incident X-ray beam greatly exceeds the range of reflection of the perfect crystal). In Figure 3 are seen topographic images of the elastic strains around the edges

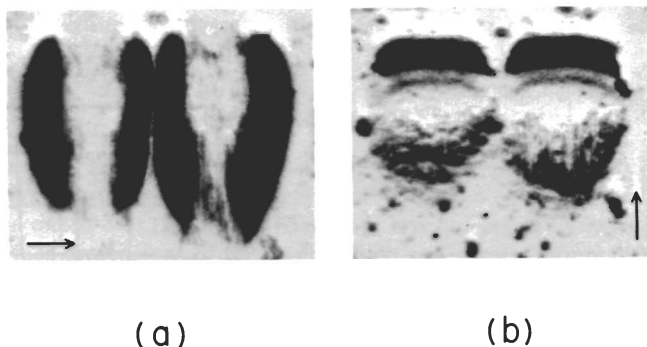


Figure 3. X-ray transmission topographs of elliptical abrasion patches on the (111) face of a natural diamond; Mo $K\alpha$ radiation; (a) $2\bar{2}0$ and (b) 220 reflections; the arrows denote \mathbf{g} vectors; the mean diameter of patches is $220\ \mu\text{m}$; and $\delta \sim 1$ to $10\ \mu\text{m}$.

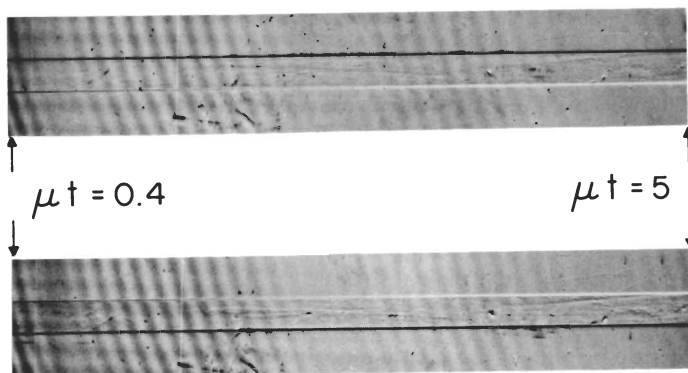


Figure 4. X-ray transmission topographs of a silicon wedge with an aluminum strip evaporated onto the X-ray exit surface; the arrows indicate values of μt at each end of wedge; the surface plane is closely parallel to (111); Mo $K\alpha$ radiation, $2\bar{2}0$ (top) and 220 (bottom) stereopair; width $2w = 720\ \mu\text{m}$; and $\delta \simeq 0.25\ \mu\text{m}$.

of two abrasion patches on a natural octahedron surface of diamond.² Natural percussion damage gives rise to the extra specks. The second set of topographs (Figure 4) shows a stereopair⁷ of a silicon wedge onto which a strip of aluminum has been evaporated. The thickness of the wedge varies roughly linearly from $0.15\ \text{mm}$ at the left-hand side of the figure to about $1.60\ \text{mm}$ at the right-hand side. The thickness of the wedge may be inferred from the Pendellösung fringe pattern⁸ which depicts contours of equal thickness. The "fading" of the pattern every fourteenth or fifteenth fringe is a diffraction effect which has been described elsewhere.⁹ Further diffraction contrast, *e.g.*, the vertical white lines¹⁰ and the specks due to accidental surface damage, are merely pointed out here and will receive no further attention.

The nature of the diffraction contrast observed on transmission topographs depends on the thickness of the specimen. For $\mu t < 1$ (μ is the linear absorption coefficient and t is the thickness of the specimen), the contrast is always positive and insensitive to the sign of the strains. The contrast seen in Figure 3 and on the very left of Figure 4 falls into this category. Now it is well established that this type of contrast becomes zero when

$\mathbf{g} \cdot \mathbf{u}$ (\mathbf{g} is the reciprocal lattice vector) itself becomes zero, so that, with proper choice of reflecting planes, indications of the direction (but not the *sense*) of \mathbf{u} may be obtained. A survey of this kind reveals that, in all diamond and silicon specimens studied, the contrast reduces to zero at all positions on the peripheral boundaries of the bad layers where $\mathbf{g} \cdot \mathbf{n}$ is zero and reaches its maximum where $\mathbf{g} \cdot \mathbf{n}$ is a maximum (see especially Figure 3). This is in accord with the model, which predicts a state of very nearly plane strain in the plane defined by \mathbf{n} and \mathbf{x}_3 , so that \mathbf{u} is always very nearly perpendicular to the periphery.

When $\mu t \gg 1$, the contrast may be either positive or negative, or both. This condition is realized on the extreme right of Figure 4. Meieran and Blech¹ have empirically established a rule for determining the sign of the strains, and thus of force \mathbf{F} , from the asymmetry of the diffraction contrast. Their rule may be stated as follows: The peripheral contrast has net positive value where $\mathbf{F} \cdot \mathbf{n}$ and $\mathbf{g} \cdot \mathbf{n}$ have the same sign. From Figure 4, we thereby deduce that \mathbf{F} is directed outward from the strip edges, so that the bad layer is in this case in a state of residual compression. (A similar deduction is made for the diamond specimens.²)

INTERPRETATION OF CONTRAST MECHANISMS

Before we can make an estimate of the magnitude of the elastic strain field giving rise to the observed diffraction contrast on the topographs, we must first understand the contrast mechanisms themselves. In the previous section, we distinguished between contrast at low absorption (commonly termed *extinction* contrast) and contrast at high absorption (*Borrmann* contrast). A tentative inspection of Figure 4 would indicate that the distinction between these two contrast regimes is not always too clear. The edges of the strip for which $\mathbf{g} \cdot \mathbf{n}$ is positive give rise to a band of positive contrast invariant of crystal thickness, while the opposite edges give rise to a band of similar width within which the contrast changes progressively from positive to negative as the crystal becomes thicker. The striking implication to be made from this observation is that the *spatial range* of contrast is determined uniquely by the strain level and not at all by the absorption level, absorption accounting only for the *distribution* of intensity *within* the bands of contrast. Thus, if we can establish the strain situation at the extremities of the bands where the contrast becomes zero, we have a means by which the entire strain field may be specified, and this without having to place any restrictions on specimen thickness.

Unfortunately, the diffraction of X-rays in nearly perfect crystals is a very complicated process when the beam incident on the crystal is widely angularly divergent. The reason for this is that, in general, the diffracted intensity reaching each point on the crystal exit surface is composed of the sum of contributions from rays contained within the *energy-flow-triangle* delineated by the directions of the direct and diffracted beams. The relatively large angle subtended by these two directions, together with the relatively thick specimens used, generally precludes such practical simplifications as the "column" approximation made in electron microscopy. But, in certain instances, such as at very low and very high absorption, and with the strain mainly localized near the X-ray exit surface of the crystal, at least a semiquantitative analysis of the contrast can be developed. The treatment is further aided by considering only cases of symmetrical transmission so that \mathbf{g} is parallel (or antiparallel) to \mathbf{n} .

Penning and Polder¹¹ were the first to present a formal treatment of the behavior of X-ray beams in *slightly* distorted crystals. A slightly distorted crystal is interpreted as one in which the allowed wave field at each point can be completely specified by wave points on the various branches of the dispersion surface construction in reciprocal space.

Each wave point corresponds to a ray (energy-flow vector for a pair of incident and diffracted waves) whose direction of propagation is normal to the dispersion surface at that point. The Penning and Polder theory indicates that, in an undistorted crystal, the wave points retain their location on the dispersion surface as the rays pass through the crystal, while, in a slightly distorted crystal, they "migrate" along their respective branches. The physical interpretation of the wave-point migration is that the rays propagate along curved paths rather than in straight lines as they do in perfect crystals and that there is an associated redistribution of the energy flow in the incident and diffracted directions. The amount of migration of a given wave point as the ray propagates an incremental distance is proportional to a deformation parameter η defined in terms of the component of \mathbf{u} parallel to \mathbf{g} : for \mathbf{g} parallel to \mathbf{x}_2 , we have,^{11,12,13} with θ the Bragg angle and with \mathbf{x}_2 and \mathbf{x}_3 defining the plane of incidence,

$$\eta = \cos^2 \theta \frac{\partial^2 u_2}{\partial x_3^2} - \sin^2 \theta \frac{\partial^2 u_2}{\partial x_2^2} \quad (2)$$

Reversing the sign of u_2 or \mathbf{g} reverses the sign of η . The total migration of a ray when it reaches the exit surface is then proportional to the integrated value of η over the ray path between the entrance and exit surfaces. The terms $\partial^2 u_2 / \partial x_3^2$ and $\partial^2 u_2 / \partial x_2^2$ [computed from equation (1)] are shown as functions of relative depth x_3/w below the crystal surface in Figure 5. It is noted that, in all cases, these terms reverse their sign just beneath the crystal surface and that they attain their maximum value *at* the crystal surface.

We now investigate the application of the above concepts to the strain field at the edges of the evaporated aluminum strip on the silicon substrate (Figure 4). At both high and low absorption, it will be found that the observed contrast can only be explained in terms of a breakdown of the Penning and Polder theory.

High-Absorption Case ($\mu t \gg 1$)

When the absorption is high, Borrmann transmission occurs; *i.e.*, rays which belong to that branch of the dispersion surface with the longest wave vectors and which travel closely parallel to the Bragg planes show anomalously high transmission, while all remaining rays are rapidly attenuated. For the weakly absorbed rays, Penning and Polder show that, when the deformation parameter η is positive, the wave points migrate along the dispersion surface in such a way that the flow of energy into the diffracted beam becomes increased (at the expense of the direct beam); similarly, for a negative parameter, energy is transferred into the direct-beam direction. The integration of η is now performed by making the assumption that the ray-propagation vector remains antiparallel to \mathbf{x}_3 ; since the strongest distortion is at the X-ray exit surface, this assumption should not lead to much error owing to spreading of the rays. When this is done, it is found that the integrated value of η at the exit surface is zero for all values of x_2 . This is not altogether

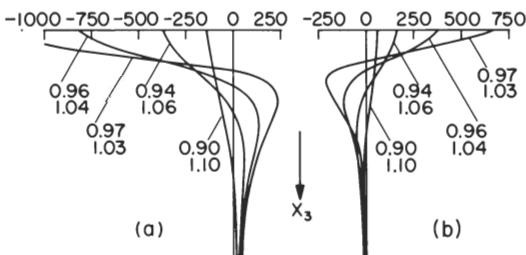


Figure 5. Plots of (a) $\partial^2 u_2 / \partial x_3^2$ and (b) $\partial^2 u_2 / \partial x_2^2$ (plotted on abscissas in units of $F'/E\tau^2$) as a function of relative depth x_3/w (plotted down to the depth $x_3 = 0.12\tau$); labels on the curves denote particular values of x_2/w .

surprising since we saw in Figure 5 that the terms in η reversed their signs below the crystal surface. The physical interpretation of the zero integral is best seen with reference to the first of the two terms in equation (2). The integration of this term over the thickness of the specimen along x_3 gives, for small θ , the difference in lattice tilt at the exit and entrance surfaces. Both these tilts must be zero according to the model of Figure 2 in which the surfaces are flat and stress free except at the peripheries of the bad layer. Thus the Penning and Polder theory would predict zero contrast, which is, of course, in direct contradiction with the observation in Figure 4.

The explanation of this apparent discrepancy lies in the fact that we have assumed the lattice distortion to be small enough that the behavior of X-rays in the crystal may be represented by a migration of wave points along the branches of the dispersion surface. However, Penning¹² shows that, when $|\eta|$ locally exceeds some critical value $|\eta_c|$, the propagating ray can no longer adjust its curvature sufficiently rapidly to satisfy the above dynamical description (see later). Bearing this in mind, we now investigate the possible behavior of a ray approaching the exit surface in Figure 2. We find from Figure 5 that, at the edge for which \mathbf{g} is parallel to \mathbf{n} , the integrated value of η will first become increasingly positive, reaching a maximum value where the curves cross the ordinate, and will subsequently decrease again toward zero. If $|\eta_c|$ is exceeded before reaching the exit surface, the ray can no longer be dynamically scattered and will pass out of the crystal without further reflection. This will prevent the integrated η from attaining its zero value, so that the *net* η will be effectively positive at the exit surface and will thus give rise to extra intensity in the diffracted-beam direction. Similarly, with \mathbf{g} antiparallel to \mathbf{n} , the sign of η becomes reversed, so that, for the opposite edge of the strip, extra intensity will appear in the direct- rather than diffracted-beam direction. This explains the asymmetric contrast on the right-hand side of Figure 4.

Low-Absorption Case ($\mu t < 1$)

The low-absorption case is complicated by the presence of rays from *all* points on *all* branches (including those branches due to the polarization of the beam) of the dispersion surface. However, the situation is simplified by the fact that the upper and lower branches have an equal and opposite effect on the integrated intensity at the exit surface. Therefore, we should again expect to observe zero contrast at the periphery of the bad layer. But, when absorption is low, we must take cognizance of the divergent incident beam. Only that portion of the beam falling within the angular range of reflection of the perfect crystal is dynamically diffracted according to the dispersion-surface representation, the remainder of the beam passing through the crystal almost unattenuated. It is this latter part of the incident beam which can give rise to diffraction contrast. Those regions of crystal for which $|\eta| > |\eta_c|$, although not able to diffract the X-rays dynamically, will be suitably oriented to diffract some part of the intense direct beam, which gives rise to positive contrast at *both* edges of the strip on the left-hand side of Figure 4.

ESTIMATE OF PARAMETER F

In the previous section, we saw that the diffraction contrast at high and low absorption could be explained if we postulated that the lattice distortion near the periphery satisfied the condition $|\eta| > |\eta_c|$. (The argument can be extended to the case of intermediate absorption.²) Penning¹² interprets the breakdown of the dynamical scattering concept in the following way. If the distortion of the crystal is too severe, there are insufficient

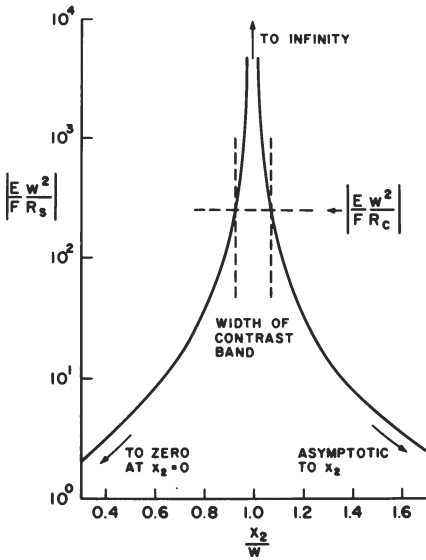


Figure 6. Plot of $|Ew^2/FR_s|$ as a function of the relative length x_2/w . The vertical dotted lines represent the limits of observed diffraction contrast and the corresponding horizontal dotted line then represents the cutoff value of $|R_c^{-1}|$.

reflecting planes to generate the necessary curvature of the ray path. Using an argument of this kind, one obtains²

$$|\eta_c| \simeq 1/gt_e^2 \tag{3}$$

with t_e an extinction distance.

For the diffraction conditions used in Figure 4, $\theta = 11^\circ$, so that the first term in equation (2) is the dominant one. We may therefore approximate η_c to R_c^{-1} , where R is the radius of curvature of the Bragg planes. Now, we saw in Figure 5 that this curvature attained its maximum value R_s^{-1} at the X-ray exit surface. Thus, for diffraction contrast to appear, the curvature $|R_s^{-1}|$ should exceed the critical value $|R_c^{-1}|$ computed from equation (3). In Figure 6, $|R_s^{-1}|$ is plotted as a function of x_2 (the quantities E , F , and w appear when the curvature is plotted in dimensionless form). From the position of the contrast band at the aluminum strip edges marked on this diagram, we find

$$\left| \frac{1}{R_c} \right| = 2.5 \times 10^2 \left| \frac{F}{Ew^2} \right| \tag{4}$$

as the critical curvature relevant to Figure 4. Equating the right-hand sides of equations (3) and (4) and inserting $E = 13 \times 10^{11}$ dyne/cm² for silicon, $2w = 0.072$ cm, $g = 5.2 \times 10^7$ cm⁻¹, and $t_e = 37 \times 10^{-4}$ cm for Mo $K\alpha$, 220 reflection in silicon, we arrive at a value of 1×10^4 dyne/cm for F . This may be compared with the value $F = 5 \times 10^5$ dyne/cm obtained for the abrasions on the diamond surface in Figure 3.²

CONCLUSION

We have presented an elastic model from which the strains around damaged layers of crystal surface may be calculated, and it has been shown that the single parameter F characterizing the strain field can be determined from X-ray topographs by simply observing the spatial range of diffraction contrast. It is, however, pointed out that several approximations attend the treatment given above. For instance δ is considered effectively infinitesimally small so that we can introduce the concept of the line force \mathbf{F} in the surface. In the cases discussed above, the width of the contrast bands greatly exceeds δ ,

so that little error is introduced. We also considered θ small so that η_c might be replaceable by R_c^{-1} ; for θ larger, Figure 6 would require R_s^{-1} to be replaced by η_s , and this plot would then only be valid for the one value of θ . It was further assumed that the curvature of the rays through the distorted crystal was not severe; the small θ and the localization of the strain field at the exit surface permitted this assumption to be made. Finally, the Penning criterion predicting the breakdown of dynamical scattering [equation (3)] is not exact and is subject to some degree of uncertainty. Thus, in applying the above treatment to the evaluation of crystal surface strains, one must ensure that the various assumptions are adequately satisfied, and the deduced value of F must be regarded as having order of magnitude accuracy only.

ACKNOWLEDGMENTS

The author wishes to point out that parts of this work were carried out in collaboration with Professor F. C. Frank, Dr. M. Hart, Dr. A. R. Lang, all of Bristol University, and Dr. E. M. Wilks, of Oxford University. He also wishes to thank Professor Barton Roessler, of Brown University, for useful criticisms of the manuscript. He is indebted to Industrial Distributors and the Advanced Research Projects Agency for financial support.

REFERENCES

1. E. S. Meieran and I. A. Blech, "X-Ray Extinction Contrast Topography of Silicon Strained by Thin Surface Films," *J. Appl. Phys.* **36**: 3162, 1965.
2. F. C. Frank, B. R. Lawn, A. R. Lang, and E. M. Wilks, "A Study of Strains in Abraded Diamond Surfaces," *Proc. Roy. Soc. (London)* **A301**: 239, 1967.
3. K. Martin, "Irradiation Damage in Lithium Fluoride," Thesis, Bristol University, 1966.
4. J. M. Fairfield and G. H. Schwuttke, "Precipitation Effects in Diffused Transistor Structures," *J. Appl. Phys.* **37**: 1536, 1966.
5. L. D. Landau and E. M. Lifshitz, *Theory of Elasticity*, Pergamon Press, London, 1959, pp. 26-29.
6. S. Timoshenko and J. N. Goodier, *Theory of Elasticity*, McGraw-Hill Book Company, New York, 1951, pp. 85-91.
7. A. R. Lang, "Studies of Individual Dislocations in Crystals by X-ray Diffraction Micro-radiography," *J. Appl. Phys.* **30**: 1748, 1959.
8. N. Kato and A. R. Lang, "A Study of Pendellösung Fringes in X-ray Diffraction," *Acta Cryst.* **12**: 787, 1959.
9. M. Hart and A. R. Lang, "The Influence of X-ray Polarization on the Visibility of Pendellösung Fringes in X-ray Diffraction Topographs," *Acta Cryst.* **19**: 73, 1965.
10. M. Hart and A. R. Lang, "Direct Determination of X-ray Reflection Phase Relationships through Simultaneous Reflection," *Phys. Rev. Letters* **7**: 120, 1961.
11. P. Penning and D. Polder, "Anomalous Transmission of X-rays in Elastically Deformed Crystals," *Phillips Res. Rept.* **16**: 419, 1961.
12. P. Penning, "Theory of X-ray Diffraction in Unstrained and Lightly Strained Perfect Crystals," Thesis, Technological University of Delft, 1966.
13. M. Hart, "Dynamic X-ray Diffraction in the Strain Fields of Individual Dislocations," Thesis, Bristol University, 1963.